A Random Sampling-based Approach to Goal-directed Footstep Planning for Humanoid Robots

Conference Paper · August 2009

DOI: 10.1109/AIM.2009.5230019 · Source: IEEE Xplore

5 authors, including:

Zeyang Xia
Chinese Academy of Sciences
36 PUBLICATIONS **84** CITATIONS
SEE PROFILE

Jing Xiong
Chinese Academy of Sciences
20 PUBLICATIONS **60** CITATIONS
SEE PROFILE

Zhao Qunfei
Shanghai Jiao Tong University
34 PUBLICATIONS **78** CITATIONS
SEE PROFILE

Ken Chen
Albert Einstein College of Medicine
94 PUBLICATIONS **438** CITATIONS
SEE PROFILE

2009 IEEE/ASME International Conference on Advanced Intelligent Mechatronics
Suntec Convention and Exhibition Center
Singapore, July 14-17, 2009

Design and Clinical Application of the Interventional Robot THMR-I

Jing Xiong[1,2], Ken Chen[1,2], Zeyang Xia[1], Xiangdong Yang[1,2], and Ping Liang[3]
[1] Department of Precision Instruments and Mechanology, Tsinghua University, Beijing, China
[2] State Key Laboratory of Tribology, Tsinghua University, Beijing, China
[3] Department of Ultrasound, The Chinese PLA General Hospital, Beijing, China
jingxiong@ieee.org kenchen@tsinghua.edu.cn

***Abstract*— An ultrasound-guided interventional robotic system includes the image navigation system, the interventional robot, and the electro-magnetic tracking unit, among which the interventional robot is a key issue affecting the therapy effect of the interventional therapy. According to the requirements of the clinical interventional therapy, an interventional robot, THMR-I, is designed. The robot combines the SCARA structure and the serial wrist to realize the wide angle active locating and puncture. This paper describes the design aspects of THMR-I concerning the medical functionality, Safety and reliability. The accuracy of the robot system is specifically analyzed theoretically and experimentally. THMR-I has been applied in over ten cyst puncture surgeries, including hepatic cysts and renal cysts, and achieved desired therapy effects, which verified the system's design concepts, reliability, and accuracy.**

I. Introduction

Interventional therapy has experienced a rapid progress in the medical field for two decades. It is a medical technology to diagnose and treat intracorporal nidus by inserting precision instruments, such as special catheters or guidewires, with the guidance of medical images. Interventional therapy has advantages of mini-trauma, quick recovery, and low cost, so it is recognized as one of clinical medical majors with descending application values recently. Some researchers consider the interventional therapy as the third therapy technology besides internal medicine and surgery[1]. However, the application of present interventional therapy has the following aspects which should be improved: (a) Most of the applied interventional therapies are guided by traditional 2-D (two dimensional) images, with which it is difficult to exactly position the focal target; (b) Because there is no fixture for operating instruments, the surgeon cannot insert the operating instruments with only one trial, but gradually for several times, which decreases the therapy efficiency; (c) A guide frame to decides the inserting angles is necessary to assist inserting of the operating instruments; (d) The spatial constraints, unsteadiness and tiredness of surgeon's hand operation may affect the quality of interventional therapy; (e) Currently only very limited seasoned surgeons can perform the interventional therapies. The robotic assisting system is considered as one solution for the above problems, in which the medical robot is utilized to realize precision positioning and assist operation basing on the medical images analysis and three dimensional scenario constructions. By implementing the robotic assistive system, some critical issues in the interventional therapy, including preoperative planning, precision positioning, steady inserting, and supporting the instruments, should be improved so that the interventional therapy can be realized more precision, dexterous, and reliable.

Medical robot technology has been successfully applied in preoperative CT (Computed Tomography) or MRI (Magnetic Resonance Imaging) image-guided orthopedics and Neurosurgery[3]. However, because the distortion and displacement of viscous soft tissues happen easily, the US (Ultrasound) images have to be used to guide and monitor surgical process during the interventional therapy aimed at abdominal organs. Therefore, the US image-guided robot-assisted interventional therapy system is more complicated and is featured for the following aspects: (a) The processing and registration of US images are more difficult; (b) The requirement of real-time guidance and monitoring makes the work environment of the system more complicated; (c) Magnetic tracking device used in US image-guidance is easily interfered; (d) There are more factors to influence the system's positioning accuracy.

Hong[4] developed a US image-guided needle insertion robot with a passive arm and a needle-driving part for percutaneous holecystostomy, which realized automatic positioning in US image plane based on intraoperative images. Boctor and Taylor[5] proposed a dual-armed robotics system for intraoperative US image-guided hepatic ablative therapy which manages both US manipulation and needle guidance to overcome the problem of freehand US. However, to develop an integrated robot-assisted interventional therapy system aiming at clinical applications is still a challenging issue.

Our previous researches[6-10] constructed a US image navigation subsystem for interventional therapy which realized the 3-D (three dimensional) surgical planning preliminarily. The robotic-assisted puncture experiments with a passive robot validated the effect of the subsystem. According to the features and requirements of the US image-guided interventional therapy, this paper develops an interventional robot subsystem THMR-I which can safely and reliably realize active needle positioning based on the surgical planning information. The robotic-assisted interventional therapy system has been successfully applied in over ten cyst puncture surgeries, including hepatic cysts and renal cysts.

The rest of the paper is organized as follows: Section II describes the interventional therapy system and gives

design details of the interventional robot concerning its functionality, safety, and reliability; Section III analyzes the theoretical and experimental aspects of the robotic system accuracy; Section IV discusses the robot's applications in clinical cyst puncture surgeries; Section V concludes the paper.

II. Interventional Therapy System and The Robot Design

A. Interventional Therapy System Overview

A US image-guided interventional robotic system includes the US image system, image navigation system, tracking device, and the interventional robot. A typical clinical scenario of an interventional therapy is showed in Fig.1.

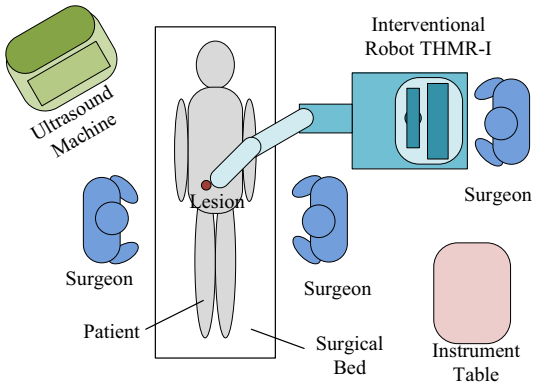

Fig. 1. The clinical scenario of an interventional system.

1) US machine: The US machine scans the celiac tissue lesions of the patient to obtain its 2-D B-type US image and transfers it to the work station. If the preoperative planning is not necessary, the image navigation subsystem can also quickly setup a 3-D model to determine the lesion target point through on-site US scanning.

2) Image navigation subsystem: The function of the image navigation unit includes 3-D preoperative planning, intraoperative positioning and navigation. The preoperative planning system constructs the 3-D model of the affected part, according to which the surgeon positions the focal target. The intraoperative positioning and navigation system maps the preoperative planning results on the patient's affected part and registers the preoperatively constructed model to the operating space.

3) Tracking device: A magnetic tracking device used in our system consists of a fixed transmitter and two receivers which can be moved freely and whose positions and orientations are tracked in the transmitter coordinate system. The transmitter is fixed to the robot base, and two receivers are fixed to a standard probe with a stylus tip and a US probe respectively. The US images can be described in the transmitter coordinate system through the US probe calibration[7], and the transmitter coordinate system can be mapped to the robot basement coordinate system through the coordinate calibration experiments(see Section III.B).

4) Interventional robot subsystem: In the robot subsystem, the tracking device and a self-designed 5-degress-of-freedom (DOF) active robot are combined to realize accurate positioning and support the surgical tool such as the puncture needle.

B. Mechanical Design of The Interventional Robot

Considering the features of the US-guided interventional therapy system, the interventional robot should be as small as possible in order not to affect operations of the surgeons and the magnetic tracking device. The interventional robot THMR-I consists of a 3-DOF robot arm and a 2-DOF robot wrist (see Fig.2 and Fig.3). The puncturing needle is mounted at the end effector of the wrist. Five DOFs are equipped to realize an exact position and orientation of the puncturing needle. The robot prototype and the magnetic tracking device are fixed on a vehicle which has a lifting platform.

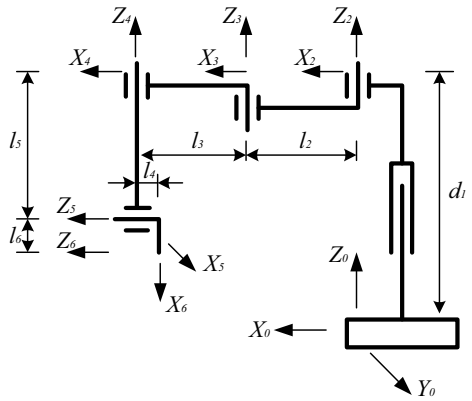

Fig. 2. The robot mechanism and its coordinate frames.

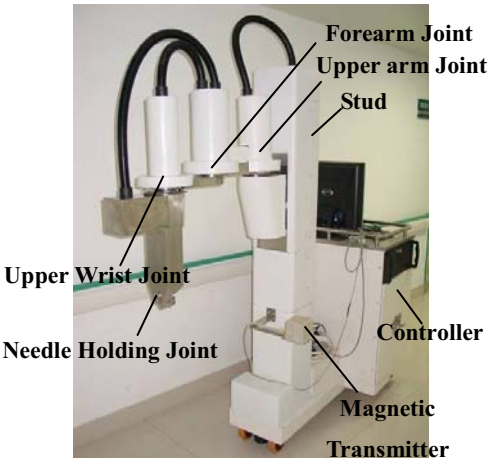

Fig. 3. The interventional robot prototype.

1) The robot arm: The robot arm is used to adjust the end effector and is realized by a SCARA mechanism, because its vertical motion and horizontal motion can be decoupled, which makes it intuitionistic to be adjusted to realize desired

end effector positions. In addition, this mechanism has high stiffness with its vertical motion and good compliance with its horizontal motion. These advantages make it very implementable in the interventional surgery. The three DOFs of the robot arm are realized by the motion of the stud, the upper arm, and the forearm.

2) The wrist: The wrist is used to adjust the orientation of the puncturing needle. It is realized by a upper wrist rotational DOF and a holding rotational DOF which are orthogonal to each other. With the above two DOFs, the wrist can rotate around the vertical axis for 270[°] and the puncturing needle has a puncturing orientation ranging from 0 to 150[°]. Compared to the manual puncturing with a fixed puncturing orientation, the robotic assisting puncturing is much more flexible and adaptive.

It is required that the puncturing pinpoint should be covered within the functional space of the magnetic tracking device, normally less than 400[mm] over the magnetic tracking device. In order to avoid the electromagnetic disturbances resulted by the robot mechanisms, motors, and reducers, the mechanical structures are made of nonmagnetic stainless steel. In addition, the holding DOF is mounted 400[mm] below its motor by applying a linkage mechanism.

C. Safety and Reliability Design

The reliability and safety of the interventional robot is not only an issue of function realization of the interventional therapy, but also an issue of safety of the patients and the surgeons. In addition to equipping spacing switches and emergency stop protection, the reliability and safety is assured by the following aspects: (a) The mechanical structure is designed with a stiffness resisting shocks of 5 [Kg]; (b) The robot can be operated in two modes, active and passive mode. The robot is operated in the active mode and can be switched timely to the passive mode in case of emergencies. While being operated in passive mode, the robot arm as well as the operating instruments can not result any harms to humans; (c) A fast and easy needle-loading/unloading mechanism is equipped at the end effector to decrease potential disturbances to the patient when it is necessary for the robot to leave the patient after puncture.

D. Active Positioning

The basement of the robot is adjusted to a suitable position and locked before the surgery starts. During the surgery, the percutaneous puncture point is selected with the standard probe by the surgeon, and the focal target is automatically computed in the image navigation subsystem. Then the above two points are mapped from the magnetic tracking transmitter coordinate system to the robot basement coordinate system to obtain the puncture position and orientation. After that, the robot actively locates the puncture needle to target orientation and the needle tip to percutaneous puncture point(see Fig.4). During the active positioning process, the real time spatial relationship between the needle and the puncturing target is displayed. The robot joints are locked once the robot reaches the desired position. Then, the surgeon begins to insert the needle, supported by the robot, according to the computed inserting depth. After the needle reaches the target position and orientation, the robot is switched to passive mode and the needle is unloaded from the robot for the succeeding therapy.

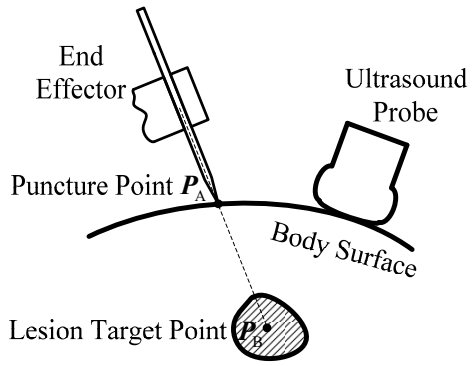

Fig. 4. Active positioning of the interventional robot.

III. Accuracy and Its Experimental Analysis

A. Analysis of System Error

What we concern during a celiocentesis is whether the puncture needle is inserted into the patient through the planned percutaneous point, and whether the puncture needle reaches the focal target. The above concerns are the basis how we assess the puncture accuracy. According to the medical accuracy requirement for celiocentesises, the final positioning error of the US guided interventional therapy should be limited within 5[mm]. According to the error transfer mechanism[10], the final positioning error of the interventional therapy system, denoted as $\boldsymbol{E}$, is resulted by the following sources: (a) random error, denoted as $\boldsymbol{E}_{\mathrm{e}}$, due to the patient's breathing, soft tissue displacement, and the doctor's puncture operation; (b) error of image navigation subsystem, denoted as $\boldsymbol{E}_{\mathrm{g}}$, due to US-image resolution and scattering, error of puncture target planning, calibration error of the US probe, and error of the magnetic tracking device(see [7] and [10] for more discussions); (c) error of transformation mapping between coordinate frames of the magnetic tracking device and the robot basement, denoted as $\boldsymbol{E}_{\mathrm{t}}$; (d) positioning error of the robot, denoted as $\boldsymbol{E}_{\mathrm{r}}$. So we have the final positioning error $\boldsymbol{E}$ as:

$$\boldsymbol{E} = \boldsymbol{E}_{\mathrm{e}} + \boldsymbol{E}_{\mathrm{g}} + \boldsymbol{E}_{\mathrm{t}} + \boldsymbol{E}_{\mathrm{r}} \tag{1}$$

$\boldsymbol{E}_{\mathrm{t}}$ and $\boldsymbol{E}_{\mathrm{r}}$ are the positioning error of the robot system. $\boldsymbol{E}_{\mathrm{r}}$ can be partly compensated by the prototype calibration. After calibration and compensation, a repositioning accuracy of 0.06 ± 0.03[mm] and an absolute positioning accuracy of 0.69 ± 0.34[mm] are realized.

B. Calibration of Coordinate Frames

The calibration of coordinate frames aims to set up the mapping relationship between coordinate frames of the magnetic tracking device and the robot basement.

Let $MC \subseteq \mathbb{R}^3$ and $RC \subseteq \mathbb{R}^3$ denote the set of points in the coordinate frame of the magnetic tracking device and the set of points in the coordinate frame of the robot basement respectively. If the transformation between MC and RC is considered as a rigid transformation, we have the mapping ψ as:

$$\psi : MC \to RC : S \in MC \mapsto \mathbf{RS} + \mathbf{p} \in RC \tag{2}$$

where $\boldsymbol{R} \in \mathbb{R}^{3\times3}$ is the spin matrix and $\boldsymbol{p} \in \mathbb{R}^3$ is the translation vector.

The calibration experiments are accomplished on a 3-D form model with benchmarking points. First, we need to obtain the coordinates of the benchmarking points in the above two coordinate frames respectively. While the robot end effecter points to the benchmarking points individually, the coordinates of the benchmarking points in the robot basement coordinate frame, $\{\mathbf{P}_1, \mathbf{P}_2, \cdots, \mathbf{P}_n\} \subset RC$, can be computed by robot forward kinematics. The coordinates of the benchmarking points in the coordinate frame of the magnetic tracking device, $\{\mathbf{S}_1, \mathbf{S}_2, \cdots, \mathbf{S}_n\} \subset MC$, can be obtained by the standard probe. Regarding the above two sets of coordinates, we have

$$\boldsymbol{P}_i = \boldsymbol{R}\boldsymbol{S}_i + \boldsymbol{p}, \quad (i = 1, 2, \cdots, n) \tag{3}$$

By implementing singular value decomposition(SVD), we obtain optimized $\boldsymbol{R}$ and $\boldsymbol{p}$ by minimizing the optimization function $f(\boldsymbol{R}, \boldsymbol{p})$, where

$$f(\boldsymbol{R}, \boldsymbol{p}) = \sqrt{\frac{1}{n}\sum_{i=1}^{n} \|(\boldsymbol{P}_i - (\boldsymbol{R}\boldsymbol{S}_i + \boldsymbol{p}))\|^2} \tag{4}$$

$\boldsymbol{E}_\mathrm{t}$ is resulted from the measurement error in the above process. The coordinate frame mapping was obtained by a calibration with 75 benchmarking points. The position error of the coordinate frame mapping is 0.81[mm] and its standard deviation is 0.53[mm].

C. Experiments on Positioning Error

The positioning accuracy of the interventional robot subsystem is tested by experiments. As shown in Fig.5(*left*), the percutaneous puncture point and the focal target is respectively simulated as two rigid needle tips fixed in the workspace with different heights. The two tips are directly selected with the standard probe and mapped to the robot basement coordinate system. The positioning errors are measured after the active positioning. The error of the puncture point is defined as the perpendicular distance from the puncture point to the puncture needle shaft, and the error of the focal target is defined as the distance between the focal target and the puncture needle tip after surgeon's puncturing. Results of 20 trials with different rigid needle positions are shown in Fig.6 and Tab.I.

The experiments show that: (a) the positioning error of the robot is a coupled result due to $\boldsymbol{E}_\mathrm{t}$ and $\boldsymbol{E}_\mathrm{r}$; (b) the positioning error of the focal target has the similar distribution as the positioning error of the percutaneous puncture point, but it is bigger than the latter. This is because the percutaneous puncture point is only affected by the positioning error of the robot structure, while the focal target is affected by not only the positioning error of the robot structure, but also the orientation error of the needle and the random error of the surgeon's operation; (c) The positioning accuracy of the robot subsystem satisfies the accuracy requirement of the celiocentesis, and furthermore it has sufficient tolerance.

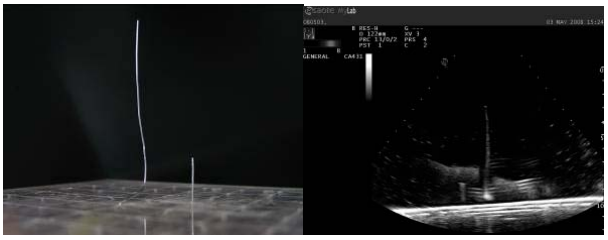

Fig. 5. Simulated puncture targets(*left*) and their US image(*right*)

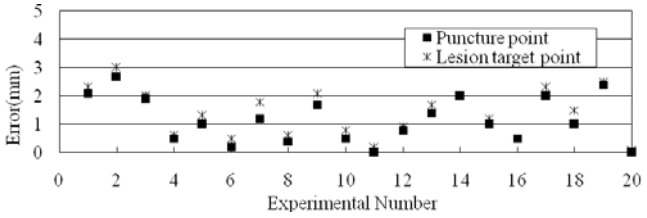

Fig. 6. Positioning accuracy of the interventional robot subsystem

D. Experiment on Integrated System Accuracy

The image navigation subsystem is integrated in this experiment, and the positioning accuracy of the integrated robot-assisted interventional therapy system is tested. The two rigid needle tips are fixed in a water tank and their US images are obtained(see Fig.5 (*right*)). The two tips are selected and identified in reconstructed 3-D model: the higher one is regarded as percutaneous puncture point, and the lower one as the focal target. Then the robot is located to the puncture position and orientation. Results of 20 trials with different rigid needle positions are shown in Fig. 7 and Tab.I.

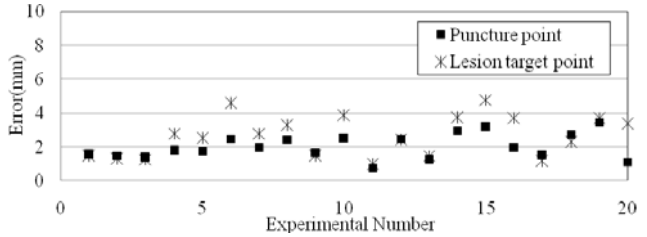

Fig. 7. Positioning accuracy of the integrated system

The experiments show that: (a) The system error ascends after the image navigation subsystem is integrated, however, the system still satisfies medical requirements for positioning error of the celiocentesis; (b) the puncturing target in the US-image is decided manually by the surgeon, so the random error has a higher effect after the image navigation subsystem

TABLE I

EXPERIMENTAL RESULTS

Error [mm]	Robot subsystem		Integrated system		Ox liver puncture
	Puncture point	Target point	Puncture point	Target point	Target point
Average	1.17	1.40	2.01	2.63	1.85
Standard deviation	0.82	0.84	0.73	1.20	0.87

is integrated; (c) The system accuracy is a coupled result affected by the system error of the interventional robot, the image system, and the random error of the surgeon.

E. Ox liver Puncture Experiment

This experiment tests the puncture accuracy of the robot-assisted interventional therapy system in hepatic tumor models. As shown in Fig.8, an agarose ball is buried in ox liver to simulate a hepatic tumor. The percutaneous puncture point is selected with the standard probe by the surgeon. The agarose ball is identified from the US images and the focal target is automatically calculated in image navigation subsystem.

In this experiment, the force to the ox liver during puncturing may cause the displacement of the agarose ball, and the contour of the ball in US images is clearer and easier identified than the rigid needle tip in the previous experiment. Generally speaking, the ox liver puncture experiment is more similar to actual clinical situation. Results of 20 trials satisfy the clinical required accuracy(see Fig.9 and Tab.I).

Fig. 8. Simulated lesion in ox liver (*left*) puncture result in a US image(*right*)

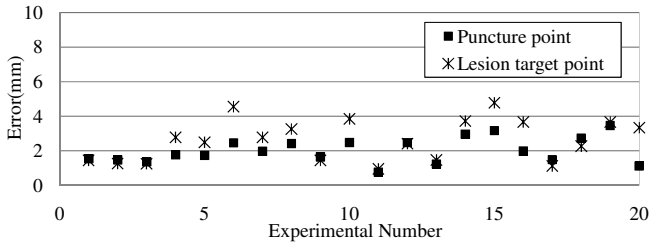

Fig. 9. Positioning error distribution of the focal target in ox liver experiment

IV. Clinical Cyst Puncture Surgeries

Before the interventional robot system is applied in clinical cyst puncture surgeries, plenty of previous experiments and preparation work have been arranged, including water tank simulation, ox liver simulation, animal experiment, and human body simulation. The water tank and ox liver simulations mentioned above verified that the system accuracy satisfies the clinical requirements. Furthermore, puncture surgeries to pigs and simulative puncture experiments to volunteers ensure the safety and availability of the system in clinical applications.

A. Surgical Procedure

The mission of THMR-I in cyst puncture surgery is to locate the puncture needle to the objective position and orientation, and to support the needle when the surgeon inserts it into the cyst. After puncturing, the surgeon unloads the needle from the robot and pushes the robot arm away so that other therapy procedures, including drawing the cystic fluid and injecting absolute alcohol, can be implemented. Fig.10 shows the actual work procedure of the robot, and Fig.11 gives snapshots of some surgical scenes.

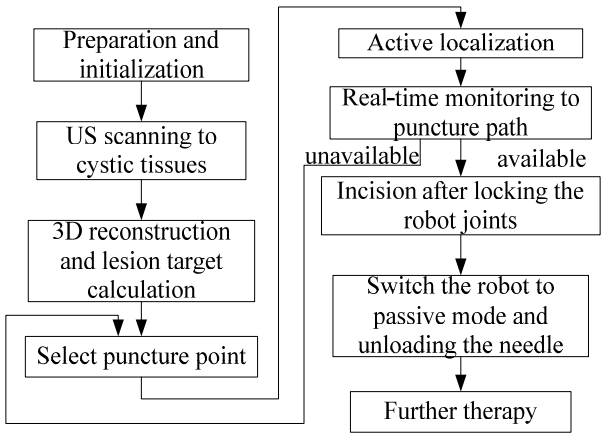

Fig. 10. Robot work procedure in clinical cyst puncture surgeries.

B. Surgical Results

By far THMR-I has been successfully applied in over ten cyst puncture surgeries including hepatic cysts and renal cysts with diameters of 5-8[cm]. Each surgery was successfully completed in about 30 minutes, and the robot-involved procedure was finished in about 10 minutes. The treatment effects and postoperative recoveries of all the patients are quite satisfying.

V. Conclusion

Interventional robot is the key issue which affects the curative effect of the interventional therapy system. According to the clinical requirements of interventional therapies, an interventional robot, THMR-I, is designed. The clinical implementations in cyst therapy verified that THMR-I satisfies the medical requirements in aspects of accuracy, reliability,

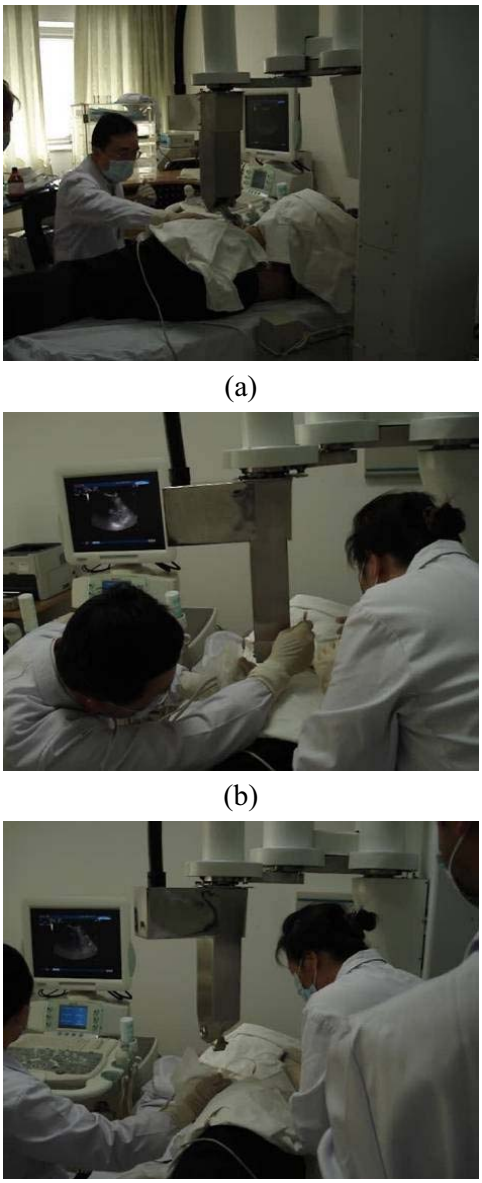

Fig. 11. Interventional surgical scenes: (a) Active localization by the robot; (b) Puncturing supported by the robot; (c) To push the robot arm away and implement further therapy

and safety. Our future works will focus on development of the real-time registration and the robot-assisted surgical planning to improve the assistant ability of the system for some more complicated and difficult surgeries such as the coagulation therapy of hepatic tumors.

ACKNOWLEDGMENTS

This work was supported in part by the National Natural Science Foundation of China (NSFC) under grant No. 50675109 and grant No. 30672016.

REFERENCES

[1] Kazanzides P, Fichtinger G, Hager G D, et al. Surgical and interventional robotics - Core concepts, technology, and design. IEEE Robotics and Automation Magazine, 2008, 15(2): 122-130.
[2] Liang P, Dong B W, Yu X L, et al. Prognostic factors for percutaneous microwave coagulation therapy of hepatic metastases. American Journal of Roentgenology, 2003, 181(5): 1319-1325.
[3] Liu D, Wang T M, Wang Z G, et al. Study on robot-assisted minimally invasive neurosurgery and its clinical application. Proceedings of the IEEE International Conference on Robotics and Automation[C]. Piscataway, NJ, USA: IEEE, 2001. 2008-2013.
[4] Hong J, Dohi T, Hashizume M, et al. An ultrasound-driven needle-insertion robot for percutaneous cholecystostomy. Physics in Medicine and Biology, 2004, 49(3): 441-455.
[5] Boctor E M, Fischer G, Choti M A, et al. A dual-armed robotic system for intraoperative ultrasound guided hepatic ablative therapy: A prospective study. Proceedings of the IEEE International Conference on Robotics and Automation. Piscataway, NJ, USA: IEEE, 2004. 2517-2522.
[6] Luo Y Y, Yang X D, Zhu S Q, Xu J, Chen K. Destination Planning and Space Mapping in the Robot-aided Coagulation Therapy System[A]. Proceedings of the IEEE International Conference on Intelligent Robots and Systems. Beijing, China: IEEE, 2006. 1249 1254.
[7] Xu J, Yang X D, Wu D, et al. An Efficient Needle Insertion Robotics System for Ultrasound-guided Hepatic Microwave Coagulation Therapy. In Proc. of the IEEE International Conference on Automation and Logistics. Jinan, China. August, 2007:1258-1261
[8] Xu J, Chen K, Yang X D, et al. Adaptive Level Set Method for Segmentation of Liver Tumors in Minimally Invasive Surgery Using Ultrasound Images. Proceedings of the 2007 IEEE International Conference on Bioinformatics and Biomedical Engineering[C]. Wuhan, China: IEEE, 2007. 1091 - 1094.
[9] Xu J. Research on the System Accuracy of the Ultrasound-guided Robot for Liver Cancer Coagulation Therapy. Ph.D. Dissertation. Tsinghua Univertisty, Beijing, 2007.
[10] Yang X D, Xu J, Liu S L, et al. The Error Propagation of the Ultrasound-guided Robot for Liver Cancer Coagulation Therapy. Robot, 2008, 30(5): 440-446.
[11] Chen K, Yang X D, Liu L, et al, Robot Technologies and Applications, Tsinghua University Press, Beijing, 2006.
[12] Arun K S, Huang T S, Blostein S D. Least-squares Fitting of Two 3-D Point Sets. IEEE Transactions on Pattern Analysis and Machine Intelligence, 1987, 9(5): 698-700.
[13] Eggert D W, Lorusso A, Fisher R B. Estimating 3-D Rigid Body Transformations: A Comparison of Four Major Algorithms. Machine Vision and Applications, 1997, 9(5-6): 272-290.
[14] Umeyam S. Least-squares Estimation of Transformation Parameters Between Two Point Patterns. IEEE Transactions on Pattern Analysis and Machine Intelligence, 1991, 13(4): 376-380.